The effect of liquid target on a nonthermal plasma jet - Imaging, electric fields, visualization of gas flow and optical emission spectroscopy

Please check the document version of this publication:

• A submitted manuscript is the version of the article upon submission and before peer-review. There can be important differences between the submitted version and the official published version of record. People interested in the research are advised to contact the author for the final version of the publication, or visit the DOI to the publisher's website.
• The final author version and the galley proof are versions of the publication after peer review.
• The final published version features the final layout of the paper including the volume, issue and page numbers.
Link to publication

PAPER

The effect of liquid target on a nonthermal plasma jet—imaging, electric fields, visualization of gas flow and optical emission spectroscopy

The effect of liquid target on a nonthermal plasma jet—imaging, electric fields, visualization of gas flow and optical emission spectroscopy

Vesna V Kovačević[1,4] , **Goran B Sretenović**[1] , **Elmar Slikboer**[2,3] ,
Olivier Guaitella[3] , **Ana Sobota**[2] **and Milorad M Kuraica**[1]

[1] University of Belgrade, Faculty of Physics, PO Box 44, 11001 Belgrade, Serbia
[2] Eindhoven University of Technology, EPG, Postbus 513, 5600MB Eindhoven, The Netherlands
[3] LPP, Ecole Polytechnique, Route de Saclay, 91128 Palaiseau, France

E-mail: vesna@ff.bg.ac.rs

Abstract

The article describes the complex study of the interaction of a helium plasma jet with distilled water and saline. The discharge development, spatial distribution of the excited species, electric field measurement results and the results of the Schlieren imaging are presented. The results of the experiments showed that the plasma–liquid interaction could be prolonged with the proper choice of the gas composition between the jet nozzle and the target. This depends on the gas flow and the target distance. Increased conductivity of the liquid does not affect the discharge properties significantly. An increase of the gas flow enables an extension of the plasma duration on the liquid surface up to 10 μs, but with a moderate electric field strength in the ionization wave. In contrast, there is a significant enhancement of the electric field on the liquid surface, up to 30 kV cm^{-1} for low flows, but with a shorter time of the overall plasma liquid interaction. Ignition of the plasma jet induces a gas flow modification and may cause turbulences in the gas flow. A significant influence of the plasma jet causing a mixing in the liquid is also recorded and it is found that the plasma jet ignition changes the direction of the liquid circulation.

Keywords: plasma–liquid interaction, electric field, Stark polarization spectroscopy, emission spectroscopy, Schlieren imaging, helium plasma jet, liquid target

(Some figures may appear in colour only in the online journal)

1. Introduction

Nonequilibrium low-temperature atmospheric pressure discharges have a wide range of applications, from environmental purposes, over synthesis of high-value materials to the field of medicine. Atmospheric pressure plasma jets (APPJs) have been one of the most studied nonthermal discharges in the past decade [1, 2]. The most prominent applications of APPJ are in the field of plasma medicine, where numerous studies have

been performed and still attract the attention of many research groups [3] in the fields of physics, chemistry and biology. Living tissue interaction with plasma is of key importance for the understanding and optimization of healing processes [2, 4]. Living tissue mainly consists of water, thus such a type of interaction could be approximated by plasma–liquid interaction. Recent studies revealed that the majority of the key chemical species for plasma medicine are generated in the gas phase [5] i.e. inside the capillary and in the effluent of the plasma jet. The production efficiency of a chemical species is a direct consequence of the physical properties of the

discharge itself. In addition, there have been recent articles presenting modeling outcomes of the influence of the liquid target on the plasma jet parameters such as electron density, electron temperature and the electric field distribution [6–8].

The aim of this work is to give a physical explanation of recent measurement results for chemical species production and also to experimentally confirm the newest modeling predictions. The article presents results of the spatio-temporally resolved imaging of the helium plasma jet–liquid target interaction. Distributions of the emissions of several excited chemical species are measured in order to identify the main excitation mechanisms. Utilizing the method of Stark polarization spectroscopy, the electric field strength distribution in a helium plasma jet interacting with a liquid target is also obtained and compared with the case of free expanding plasma jet. The electric field strength is proven to be one of the most important plasma jet parameters, which is recognized by many research groups who put effort into developing new or adopt existing methods for the electric field determination in various types of nonthermal plasma jets [9–14]. Measurements are supported by simultaneous Schlieren imaging of both the effluent of the plasma jet and the water target.

It was previously shown that, for a constant gas flow rate, the distance between the liquid target and the plasma jet nozzle influences the production of active chemical species such as OH radicals [5]. In addition, for a fixed plasma jet–liquid target distance, a change of the gas flow rate influences the plasma jet structure and footprint on the liquid target [15]. After the exit from the dielectric tube, the ionization wave is developing at the interface between the helium flow and ambient air. It has a volume trajectory that follows the 98%–99% helium-air mole fraction line, the boundary of the so called 'helium core' [16–19]. The ionization wave has an annular structure, which contracts during the propagation due to the air diffusion into the helium and shift of the mentioned 98%–99% helium-air mole fraction line towards the plasma jet axis. The ionization wave propagation is influenced by the presence of the target and the nature of the interaction depends on the target properties, the distance of the surface from the tube exit and the position of the electrical ground [20–22]. A metallic target present downstream from the helium flow may increase the maximal velocity of the streamer up to four times and double the peak electric field strength [23]. When the target is made of a dielectric material, it was shown that an increase of the permittivity of the material causes an increase of streamer parameters such as velocity, electric field strength, electron temperature and electron impact ionization source [6]. In the vicinity of the surface, a luminous sheath appears, probably as a consequence of the electric field enhancement, as was shown in the case of a solid dielectric target [24, 25]. The present work focuses on a detailed study of the plasma jet impinging the liquid surface. In order to emphasize the complexity of the plasma jet–liquid target interaction, two parameters were changed: the distance between the plasma jet and the liquid surface and the gas flow rate.
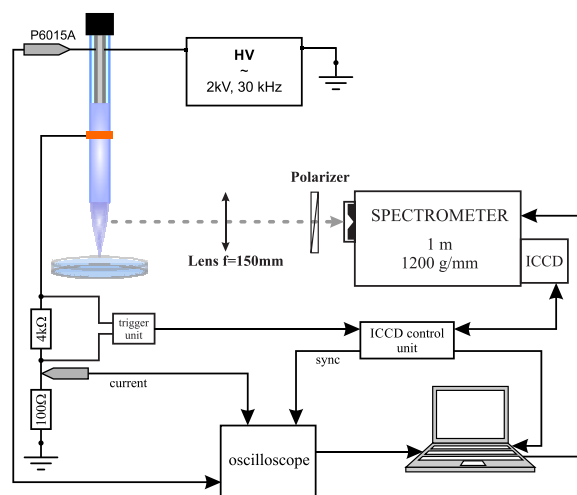

Figure 1. Schematics of the measurement setup for Stark polarization spectroscopy [26].

2. Experimental setup

The atmospheric pressure helium plasma jet used in this study has been described in detail in our previous articles [10, 25–27]. The plasma jet is configured coaxially with a high-voltage electrode centered inside a Pyrex tube (2.5 mm inner diameter, 4 mm outer diameter) and a grounded ring electrode (3 mm width) placed around the glass tube, positioned 5 mm downstream from the powered electrode. The distance from the grounded electrode to the exit of the glass capillary is 19 mm [26]. Helium (Messer, 99.996% purity) is introduced through the inner tube electrode made of stainless steel (0.8 mm inner diameter, 1.6 mm outer diameter). The gas flow is controlled by a Bronkhorst® mass flow controller in the range of 700–2000 standard cubic centimeters per minute (SCCM). The jet is powered by a sinusoidal high voltage with amplitude of 2 kV and 30 kHz frequency. Electrical parameters are measured with the oscilloscope Lecroy Waverunner 610Zi (1 GHz, 20 Gs s^{-1}), which operated in sample mode. The voltage was measured with a Tektronix P6015A high-voltage probe and the current was measured via a 100 Ω non-inductive resistor connected in series with the grounded electrode. Liquid samples are set in a Petri dish and three distances are used between the glass capillary and the liquid surface, i.e. 5, 7 and 10 mm, see figure 1. Distilled water and physiological saline (NaCl solution 0.85%) are used as targets. The liquid surface acts as a floating electrode during the interaction with the plasma jet.

The dynamics of the propagation of the ionization waves in the tube, air and its interaction with the liquid surface is monitored with an iCCD (Andor iStar) camera with a 1024 × 1024 pixel chip. For space-resolved spectroscopic measurements, the plume of the plasma jet is projected with an achromatic lens (150 mm focal length) on the slit of a 1 m spectrometer (Solar MSDD 1000) with a 1200 g mm^{-1} diffraction grating in a 1:1 ratio. Emitted light is polarized in the axial electric field direction (π polarization) by a plastic polarizer and detected using an iCCD (PI-MAX2, Princeton Instruments) with 1024 × 1024 pixels. The slit width was kept at 70 μm, which resulted in an instrumental half width of 0.051 nm, and the
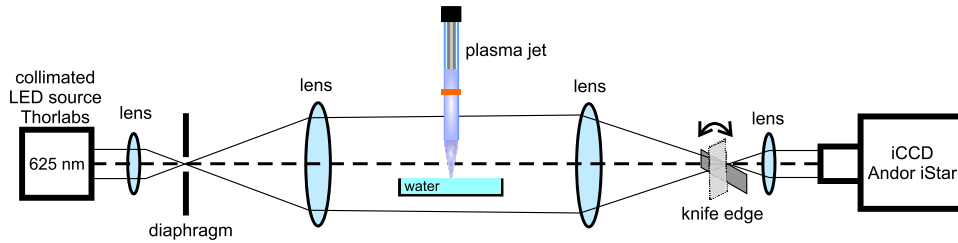
Figure 2. Experimental setup for Schlieren imaging.

spatial resolution was 12.5 μm/pixel. The iCCD was synchronized with the current signal using an external trigger unit and each image was obtained with 90 accumulations and 100 000 exposures per accumulation. Stark polarization spectroscopy, a non-perturbing method based on the Stark effect of helium lines developed by Kuraica and Konjević [28], is used for the measurements of the electric field strength distribution. Basically, Stark splitting and shifting of the allowed He I line at 492.19 nm (2^1P-4^1D) and forbidden He (2^1P-4^1F) line depend on the value of the external electric field. Measurement of the distance between these lines enables evaluation of the electric field. More details about this method and the applied procedures can be found in our previous publications [9, 23, 26, 29].

For Schlieren imaging, a simple two-lens system is used [30], with two lenses of 45 cm focal length, a high-power LED source at 625 nm, a knife edge blade and an Andor iStar iCCD camera for recording the Schlieren images. In addition, two lenses and a diaphragm were used for focusing and adjustments, as shown in figure 2. The images are taken with the blade at the focal point of the second lens with an exposure time for every image of 33 μs i.e. one voltage period. Two orientations of the blade enabled the observation of the change of gas density in two directions. In order to observe the interaction of the gas flow and the plasma plume with the liquid, a rectangular glass vessel with plane-parallel sides was constructed as a liquid container.

3. Results and discussion

3.1. Time-resolved plasma development in the APPJ and the influence of the liquid target

Electrical properties of the investigated plasma jet interacting with the distilled water positioned 7 mm from the capillary tube nozzle and with a helium flow of 1000 SCCM are presented in figure 3. As shown in figure 1, the current is measured at the ground. Every positive voltage half-cycle is characterized by one strong current peak, marked as '1' in figure 3, originating from the primary asymmetric dielectric barrier discharge ignition between the bare high-voltage electrode and glass-covered grounded electrode [25, 27]. A negative current peak, marked as '2' in figure 3, is much smaller, but substantially wider [25]. Besides these usual appearances, a small current peak is observable about seven microseconds after the positive current peak, marked as '3' in figure 3. Such an occurrence does not appear in the case of a free expanding plasma jet [27], but it is noted when the target is made of a
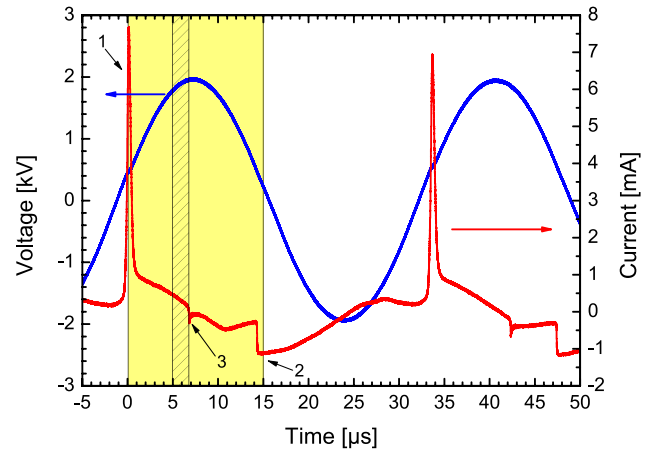

Figure 3. Applied voltage and current measured at the ground for a target distance of 7 mm and a gas flow of 1000 SCCM. The colored rectangle marks the period of the discharge development in the part of the tube and in the gap and the interval of the spatio-temporally resolved measurements of the plasma jet emission development. The smaller, patterned rectangle corresponds to the ionization wave propagation and represents the gate width of the spectroscopic measurements.

solid dielectric [25]. The sign of current peak '3' is opposite to the main current peak and corresponds to the moment when the ionization wave reaches the target. Similar electrical characteristics are recorded for all sets of conditions and the only notable difference is in the position of current peak '3' due to the different velocities of the ionization waves for different target distances and flows. The yellow-colored rectangle in figure 3 corresponds to the interval of the spatio-temporally resolved measurements of the plasma jet emission development. A different recording interval is selected for every experimental condition, i.e. different gas flows and target distances. The results are presented in figures 4–7. Spatio-temporally-resolved emission measurements that correspond to the smaller rectangle window in figure 3 are presented in figure 5. A smaller patterned rectangle matches the ionization wave propagation between the end of the nozzle and the target. The ionization wave starts its development under the grounded electrode during the moment of the positive current peak maximum.

The following figures in the subsection demonstrate the tremendous differences in discharge properties caused only by nonelectrical parameters: gas flow rate and distance between the capillary and the target. All figures are recorded with 100 ns temporal resolution and show the ionization wave transfer through part of the capillary, along the gap and finally the sheath development on the surface of the liquid. Every
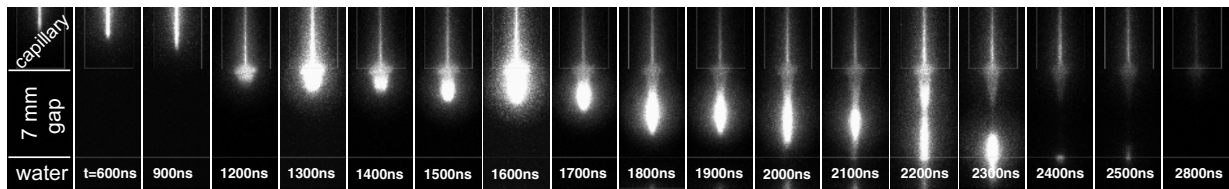
Figure 4. Spatio-temporal development of the plasma jet emission during the positive half cycle for a gas flow of 700 SCCM and a distance of the distilled water target of 7 mm. Please note that the frames are not temporally equidistant.

discharge development is recorded with more frames and here we present only the characteristic ones. Thus, the reader should be aware that the presented frames are not temporally equidistant. Figure 4 gives the recorded plasma jet luminosity development for a target distance of 7 mm and a gas flow of 700 SCCM. The discharge resembles many free expanding plasma jet characteristics; ionization wave is much faster in the gap than in the tube, it consists of a bright head and much less luminous channel behind it, while its radius decreases as it moves away from the nozzle. It crosses the gap for approximately one microsecond. When the streamer crosses the gap, a strong and luminous reconnection channel instantaneously forms between the target and the high-voltage electrode at $t = 2200$ ns, emphasizing the conductivity of the streamer channel. Then, a very weak and short cathode glow is observable in the following few hundreds of nanoseconds. Finally, the whole discharge in the observed space window lasts about 2.7 μs and radial spreading of the streamer over the water surface is not observed, which is in line with modeling predictions [7]. Namely, there is no surface charging for higher permittivity of the target, which would induce a horizontal component of the electric field that would promote a surface ionization wave. In contrast, a small permittivity enables fast charging of the surface and high electric field strength in the horizontal direction, which governs the surface ionization wave [6].

A slight alteration of the discharge conditions may considerably change the discharge properties, as presented in figure 5. Figure 5 shows the discharge development when the target is posted at the same distance as in figure 4, 7 mm away, but the gas flow is increased from 700 SCCM to 1000 SCCM, i.e. helium velocity at the exit of the tube increased from 2.4 to 3.4 m s^{-1}. Such a change increased the discharge duration from 2.7 to 9.6 μs, and the pure plasma liquid interaction duration from less than 0.5 μs to more than 7.4 μs. The development of the discharge presented in figure 5 is rather complex. A cathode-directed ionization wave strikes the liquid surface approximately 1 μs after leaving the capillary, similar to the ionization wave in figure 4, and in the exact moment when current peak '3' is detected in a current signal 7 μs after the main discharge current peak '1'. When the streamer reached the water surface, the first reconnection channel occurs, followed by a weak and short cathode glow. This occurrence corresponds to the 2900–3200 ns frames in figure 5 and roughly 10 μs in figure 3. At first sight, an irrelevant increase of the gas flow enables prolongation of the plasma liquid interaction through a second stronger reconnection channel, the 3300 ns frame in figure 5, and the formation of a longer and brighter cathode glow. In addition, a slow backward discharge front

starts to propagate towards the tube and lasts about 5 μs. At the end, the discharge vanishes through 2–3 μs of the cathode glow. Higher gas flow obviously enabled higher purity of the helium in the vicinity of the water surface for the development of a kind of transient glow discharge between the high-voltage electrode and the water surface, similar to an atmospheric dc glow discharge using a liquid electrode [31, 32]. The intensity of the cathode sheath emission is evidently weaker than the emissivity of the ionization wave head or reconnection channel, probably due to a small value of the secondary emission coefficient, which is 2–3 orders of magnitude smaller than for a metal electrode [33, 34].

In order to confirm previously presented results, additional measurements are performed with a flow of 1000 SCCM for different gaps: 5 mm, figure 6 and 10 mm, figure 7. The first conditions correspond to the low air content in helium, i.e. more extreme conditions than in figure 5. The results presented in figure 6 are indeed very similar to the results in figure 5. The discharge consists of a streamer, reconnection channel and a cathode glow with an evident slow backward discharge front. The total duration is about 10 μs. The discharge conditions of the results shown in figure 7 are similar to those presented in figure 4, i.e. they resemble higher intrusion of air in helium. As expected, the results are similar, the discharge consists of a streamer, weak reconnection and very short and weak cathode glow. The discharge development lasts about 1.9 μs. The results presented in this subsection once again underline the decisive role of the gas composition in the development of the plasma jet discharge in contact with a liquid target.

As can be seen from figure 5, the development of the plasma jet discharge in contact with the target is qualitatively similar to the single microdischarge development in a dielectric barrier discharge [35–37]. Accordingly, the plasma jet represents a suitable experimental arrangement for investigations of the discharge interaction with liquid. Namely, DBD in contact with liquid, which is widely used for the decomposition of various pollutants dissolved in water, consists of numerous temporally and spatially unstable microdischarges and their diagnostics is challenging. On the other hand, the plasma jet–liquid interaction starts with a guided ionization wave that is reproducible and stable. Its development is within the time scale that is three orders of magnitude longer than in the case of a microdischarge in air, so the use of conventional diagnostic tools, such as an iCCD camera is convenient. Also, the ionization wave develops in a much longer, centimeter scale, discharge gap. The differences between an air microdischarge and the plasma jet in contact with a target are mainly due to
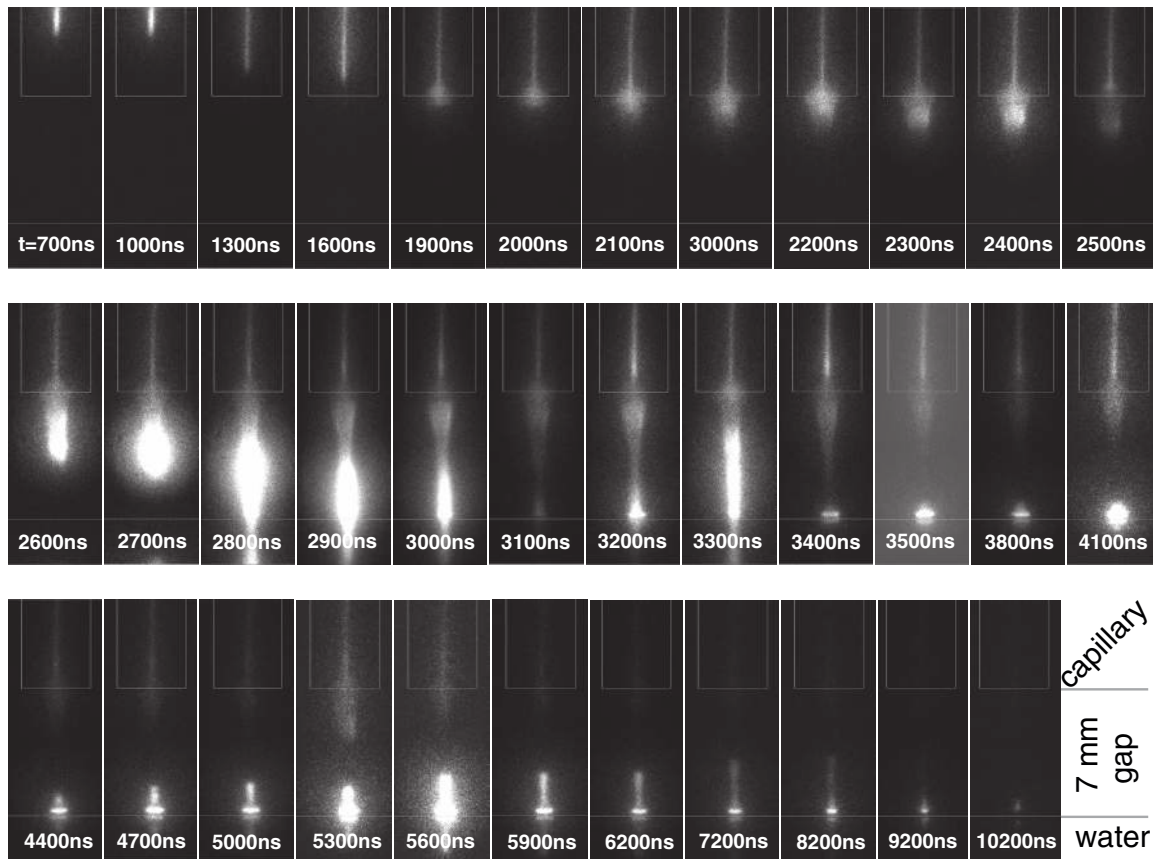
Figure 5. Spatio-temporal development of the plasma jet emission during the positive half cycle for a gas flow of 1000 SCCM and a distance of the distilled water target of 7 mm. Please note that frames are not temporally equidistant.
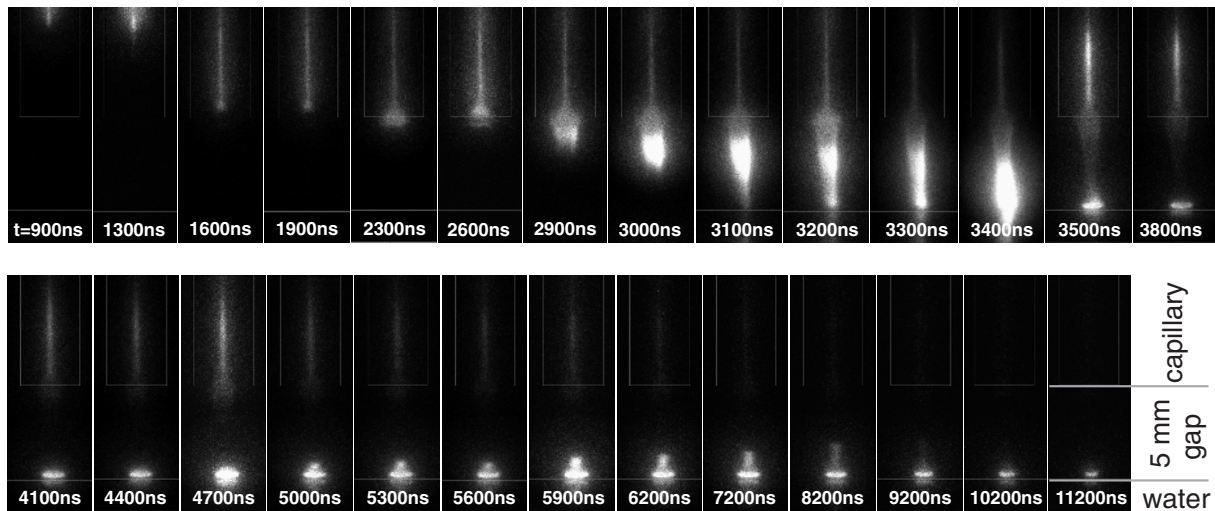
Figure 6. Spatio-temporal development of the plasma jet emission during the positive half cycle for a gas flow of 1000 SCCM and a distance of the distilled water target of 5 mm. Please note that frames are not temporally equidistant.

the different values of the first Townsend ionization coefficient, which causes lower electric fields and velocities of noble gas ionization waves.

3.2. Spatial distribution of some excited species

Electric field measurements are performed utilizing the spectroscopy of the allowed He I (2^1P-4^1D) and the forbidden He (2^1P-4^1F) line at wavelengths around 492 nm only during the ionization wave propagation between the jet nozzle and liquid target. Obtaining the spatial development of these lines enabled the investigation of the development of several transitions appearing in the same 10 nm-wide spectral window of the iCCD, see figure 8. Beside helium lines, it was possible to observe: H_β line at 486.14 nm, the nitrogen molecule second positive system (SPS) transition N_2 (C $^3\Pi_u)_{\nu'=1} \rightarrow (B^3\Pi_g)_{\nu''=7}$

Figure 7. Spatio-temporal development of the plasma jet emission during the positive half cycle for a gas flow of 1000 SCCM and a distance of the distilled water target of 10 mm. Please note that frames are not temporally equidistant.
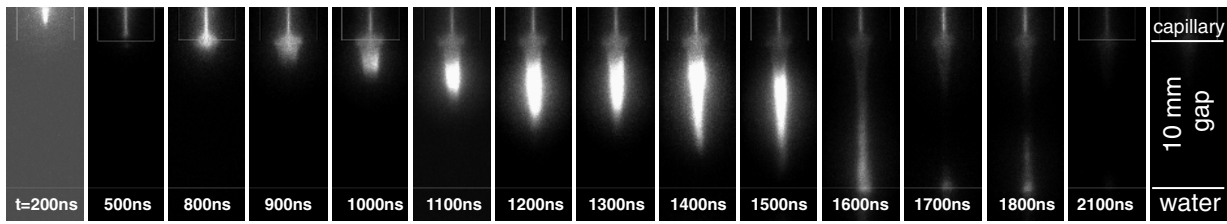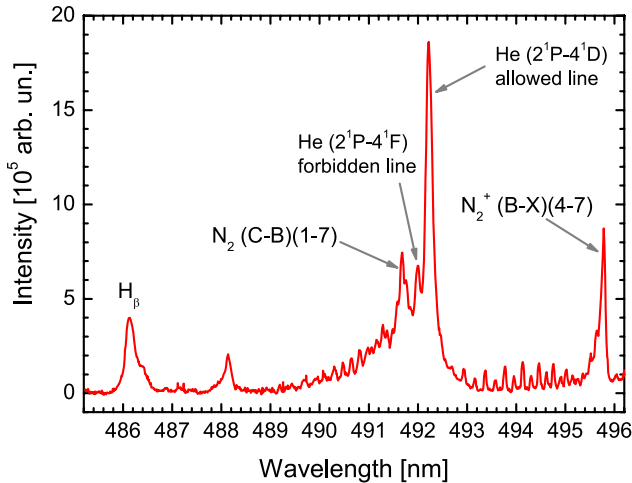

Figure 8. Part of the optical emission spectra observed during the plasma jet–liquid target interaction.

at 491.68 nm and the nitrogen molecular ion first negative system (FNS) transition N_2^+ $(B^2\Sigma_u^+)_{\nu'=4} \rightarrow (X^2\Sigma_g^+)_{\nu''=7}$ at 495.79 nm [38]. It should be noted that the polarizer was present during all spectroscopic measurements, but in the case of the emission intensity analysis, it acts only as a neutral density filter and does not affect the quality of the obtained information.

According to the dominant excitation mechanisms, four optical emissions studied in this subsection could be divided in two groups [39, 40]. The He line and the second positive system band belong to the group where direct excitation by energetic electrons is dominant, while the H_β line and the first negative system band belong to the group where metastables play a significant role in the excitation. The excited state of the nitrogen molecular ion ($E_{N_2^+(C)} = 18.7$ eV) is efficiently produced through the resonant reaction channel between metastables of helium ($E_{2\,^3S} = 19.8$ eV and $E_{2\,^1S} = 20.6$ eV) and nitrogen in the ground state in the so-called Penning ionization process. H_β appears due to energy transfer from the He metastable atoms [He(2^3S)] and molecules [He$_2(a^3\Sigma_u)$] [41], which was also confirmed experimentally for the helium plasma jet [39]. The exposure time, number of exposures and accumulations were the same for different conditions, so it was possible to compare intensities of the observed emissions and qualitatively analyze the production of excited species with dependence on the discharge conditions. The results of the space-resolved optical emission measurements of these four transitions during the ionization wave propagation are presented in figure 9. The dependencies of the spatial intensity

distributions on the gas flow for the free expanding plasma jet and the plasma jet in contact with a liquid surface, presented in figure 9, give a rough picture of the target and gas flow influence on the electric field distribution, metastable densities and finally on the production of active chemical species in the ionization wave. Also, the results of the target conductivity influence on these distributions are presented in figure 9. Similar results are obtained for target distances of 5 and 10 mm, but not presented here.

For the free expanding plasma jet, top values of all emissions are similar, but shifted in space due to the different gas compositions caused by the different helium flows. The emissions follow the trend of the electric field strength distributions published in one of our previous articles, where the maximal values of the electric field are also similar, but shifted away from the tube as the gas flow increases [26].

When the liquid target is placed 7 mm downstream from the nozzle, two scenarios are observed depending on the gas flow, see figures 4 and 5. The plasma liquid interaction is weak for the flow of 700 SCCM, and the discharge consists of a streamer and a short-living reconnection channel. The emission intensity of the He I 492.19 nm line, figure 9(a), is similar to the free expanding plasma jet case. The difference between the free expanding plasma jet and the plasma jet interacting with a liquid target is notable in the vicinity of the target when intensities of the observed transitions drop. Emissions of helium line and the SPS of nitrogen give the information about the convolution of electron density, electron energy and the density of the atoms in the ground state. The intensity of the N_2 SPS has an increase in comparison to the free plasma jet for the flow of 700 SCCM, and a maximum closer to the nozzle, which could be understood through a much lower excitation energy (11 eV) in comparison with the He line (23.7 eV). Much more interesting are the emissions of N_2^+ FNS and especially the H_β line, as these emissions are increased two and four times, respectively, only by the introduction of the target. A maximum of the intensity of these two emissions is positioned in the center of the gap, similar to the emission of the N_2 SPS. Based on the intensities of these emissions, one can conclude that the presence of the target induced an increase of the density of helium metastables. Detailed study of the influence of the conductive target on the helium metastable production is offered in [42]. It was shown that the presence of a conductive target induces an increase of the helium metastable density for one order of magnitude. These results are also in accordance with the results presented in [43], where a correlation between the N_2^+ density with the metastable density is confirmed for the positive polarity of the

J. Phys. D: Appl. Phys. 51 (2018) 065202
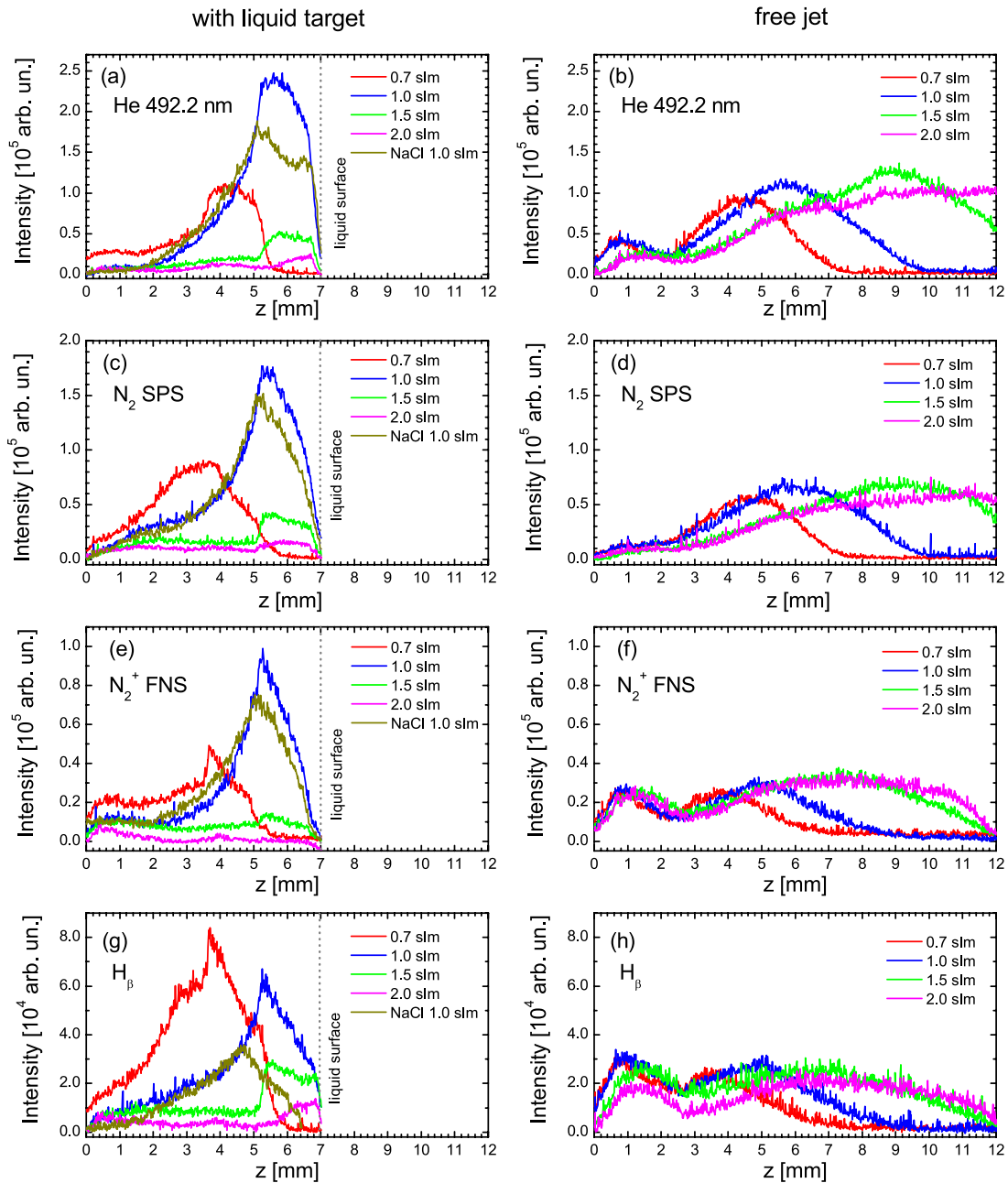
V V Kovačević *et al*

Figure 9. Spatial distributions of different emissions for the free expanding plasma jet and the plasma jet in contact with a liquid target. The target was placed 7 mm downstream from the end of the glass tube, and gas flow was changed in the range of 700–2000 SCCM. On the *x*-axis, *z* represents the distance from the tube end.

plasma jet in contact with a metallic target. The behavior of the OH band emission is shown to be very similar to the H_β line intensity distribution in the helium plasma jet interacting with a conductive target [39]. The presence of the target caused a high growth of H_β emission, which leads to the conclusion that the OH density also increases, which is in agreement with the OH density laser-induced fluorescence measurements for the free expanding plasma jets and jets in contact with different targets, including liquid ones [44]. The increase of the gas flow to 1000 SCCM causes stronger interaction between the streamer and the target, according to the intensity of most of the emissions. Also, most of the emissions are shifted towards the liquid target, which makes this set of conditions

more convenient for applications. The plasma jet properties at two gas flows, 700 and 1000 SCCM, are comparable with 'touching' and 'not-touching' plasma jet situations studied in recent publications dealing with the modeling of the plasma jet-liquid target interactions [7, 45]. These studies predicted a slight decrease of the ionization wave velocity and ionization source due to the increase of liquid conductivity. This is also observable in figure 9, where the intensities of all observed emissions decrease when a distilled water target is substituted by a physiological saline solution. Finally, a drastic increase of gas flow, 1500 and 2000 SCCM, leads to a drop of intensities of all emissions far below the free expanding plasma jet, probably due to the increased helium content and the
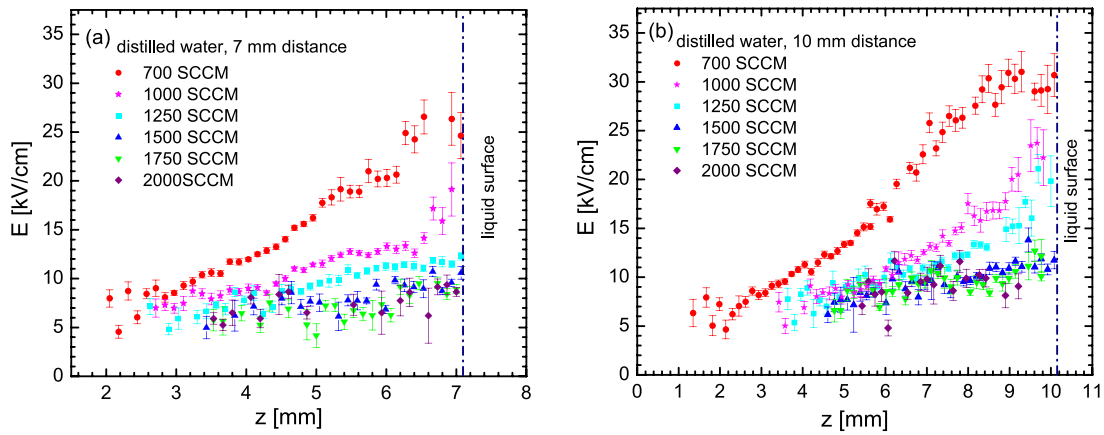
Figure 10. Electric field strength distributions in the plume of the plasma jet touching the surface of the distilled water positioned at (a) 7 mm and (b) 10 mm downstream from the glass tube for different gas flows.

turbulences in the space between the nozzle and target. Based on all mentioned observations in this subsection, very simple spectroscopic measurements can give basic information of the activity and efficiency of plasma jet–liquid target interaction, which could be used for a feedback loop system to control the plasma jet properties, as suggested in [46].

3.3. Electric field measurements

The electric field profiles in the plume of the plasma jet obtained for different helium flows when the jet interacts with distilled water placed 7 and 10 mm below the glass capillary are presented in figure 10. The graphs show an evident increase of the electric field along the jet axis for all the flows. The dramatic influence of the gas flow rate on the electric field value represents a unique feature of the plasma jet. Such an influence of a non-electrical parameter on the electric field profile in the plasma jet was also found in a freely expanding jet [26]. In the area 1–2 mm above the liquid there is an increase and saturation of the electric field for lower gas flows, compared to the profile in the major part of the gap.

For higher gas flows, no particular change in the electric field profiles could be observed in the area just above the liquid. The value of the electric field strength at the contact point increases by a factor of 3 for a change of the gas flow from 2000 SCCM to 700 SCCM. For all gas flows, the electric field reaches a peak value close to the liquid surface ranging from 8–30 kV cm^{-1}, with a distinct feature—the lower the helium flow, the higher the electric field strength. Similar profiles of the electric field are observed for 7 and 10 mm distances, but the slope of the field increase is a bit faster with a shorter distance. Electric fields in the range of 30 kV cm^{-1} measured in the head of the ionization wave near the liquid surface under some of the examined conditions may be sufficient for the electroporation of cells if their duration is higher than 60 ns [47], which is fulfilled in the case of the examined plasma jet. After the analysis of the figures that present the discharge development spatial emission of different species and the electric field strength in the head of the ionization wave under various conditions, it is clear that high electric field in the streamer head does not always mean the strongest

and longest plasma liquid interaction. From these figures, one can conclude that there are optimal conditions that can bring high electric field with high production of reactive species and an increased interaction length. In our experiment, it was for a flow of 1000 SCCM with a target placed 7 mm downstream from the nozzle. Higher helium flow means lower electric field in the streamer head. That is due to the much higher values of the first Townsend coefficient for a certain electric field in pure helium than in helium with the addition of air [26, 48, 49]. Furthermore, nitrogen ions are the main constituents of the space-charge layer and a lack of nitrogen in the flow reduces the space-charge density, and consequently the electric field strength. On the other hand, a higher He/Air ratio is favorable for a glow-like discharge development, similar to the conventional dielectric barrier discharge in helium [50]. Thus, the discharge duration extends due to the high purity helium as a medium gas. That is why a higher electric field of the ionization wave does not mean a stronger overall plasma jet–liquid target interaction.

In order to determine which parameter, gas flow or a liquid target presence, has a decisive role in the electric field distribution in the streamer head, the electric field distributions for the free expanding plasma jet and the plasma jet impinging the water surface for different gas flows are presented in figure 11. It is clear that the liquid target influences the electric field values in the case of a low gas flow and further target distances, figure 11(a)–(c). In contrast, the target does not impact the electric field strength values for higher gas flows, figures 11(d)–(f), but it obviously affects the stability and the reproducibility of the discharge according to the scattering of the experimental points. There are two types of influences of the target on the plasma jet. The first is an elongation of the plume and the second is an increase of the electric field in the vicinity of the water surface. The elongation of the plume is the consequence of the plasma–gas flow interaction, which is observed in this kind of discharge. More discussion about this phenomenon is given in the following subsection. The enhancement of the electric field strength in the vicinity of the surface layer, which is especially noticeable for the gas flow of 1000 SCCM, is a consequence of the electric potential compression against the high permittivity water layer
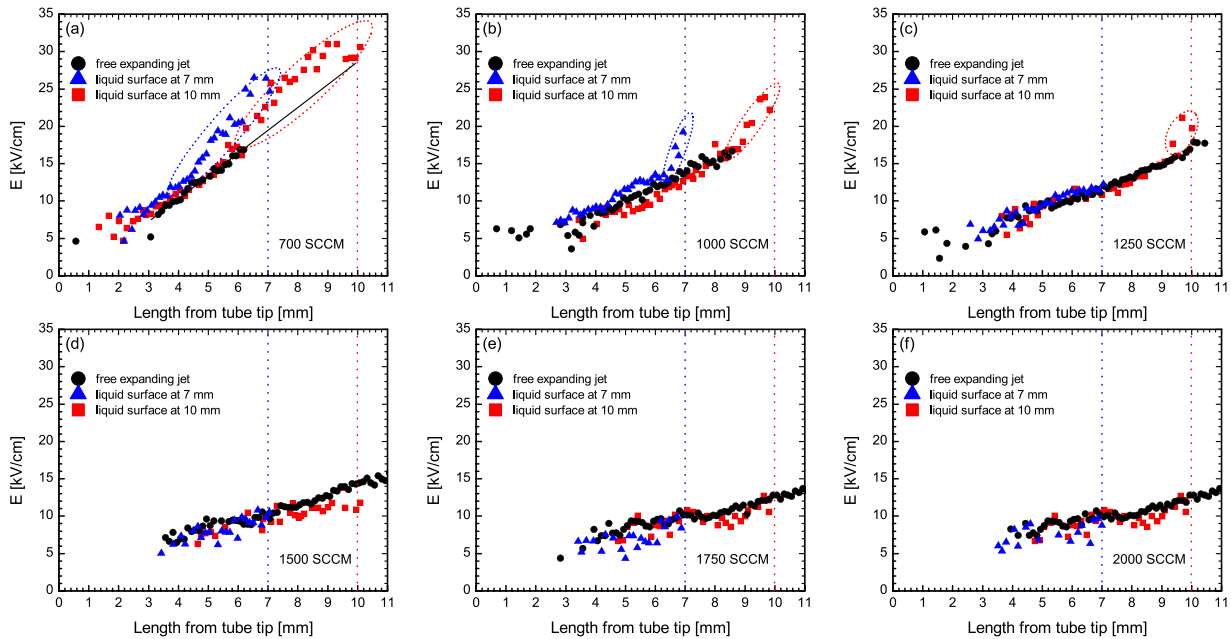
Figure 11. Comparison of the electric field strengths in the streamers of free expanding plasma jets and plasma jets interacting with targets for different gas flow rates and target distances.

and charging of the surface, as argued in [45]. For higher gas flows, there is no visible contraction of the jet on the liquid surface, thus there is no effect of the smaller volume, and the electric potential compresses on a relatively large surface, which causes less electric field enhancement. Furthermore, there is a higher scattering of the experimental points for higher gas flows and a more pronounced dimpling effect at the jet striking point to the water surface, which could block the optical path of the light, so that electric field increase detection is more challenging.

The electrical conductivity influence of the water target on the electric field distribution is also a focus of interest of this article. The dielectric constant of a solution decreases with the salt concentration and for a 0.85% NaCl solution the dielectric decrement is less than 2%, with a relative permittivity of 80 for water and 78.6 for the solution [51, 52]. The computational study of the plasma jet touching dielectric and metal surfaces showed that an increase of relative permittivity from 2 to 80 leads to an increase of the electric field which saturates by $\varepsilon_r = 80$ prior to striking the surface with a peak magnitude of $28\,\mathrm{kV\,cm^{-1}}$ [6]. The model predicts there is little difference in peak magnitudes and spatial distribution between $\varepsilon_r = 80$ and a metal surface. As was noted in the previous subsection, the increase of the water conductivity caused a slight drop of the intensity of all observed optical emissions. Modeling of the plasma jet interaction with a liquid target predicts a slightly slower ionization wave when the conductivity of the target is substantially higher than the distilled water conductivity [45]. The increased conductivity of the liquid distributes the potential along the surface more uniformly, which then reduces the vertical electric field. Nonetheless, the predicted reduction of the value of the electric field strength is not large, 10% or less at the surface of the liquid target.

In order to study the influence of the liquid conductivity on the electric field strength, the distilled water is substituted by
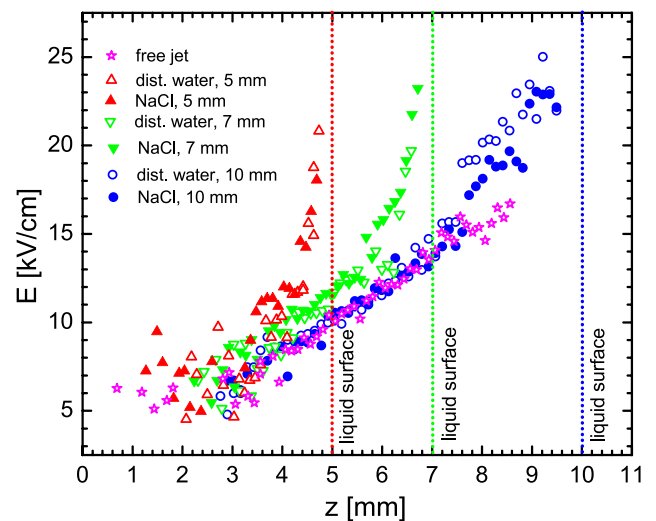
Figure 12. Electric field strength distributions in the plume of the plasma jet touching the surface of the distilled water and physiological saline solution placed at different positions from the glass tube, with a 1000 SCCM He flow.

a 0.85% NaCl solution. The electric field distributions when the plasma plume touches distilled water and NaCl solution placed 5, 7 and 10 mm downstream from the glass tube are shown in figure 12, for the 1000 SCCM flow rate. Despite the fact that the initial conductivity of distilled water was 2.5 μS cm^{-1}, while that of physiological saline was 14.94 mS cm^{-1}, measurement results for these two liquids gave the values of the electric field that are similar within the experimental errors. Thus, one can conclude that the conductivity of the liquid target does not substantially change the electric field strength in the ionization wave, which is in fair agreement with modeling outcomes.

Taking into account discrepancies between the computational configuration and experimental conditions, the

Figure 13. Schlieren images of the jet without a target for different gas flows. The exit of the vertically installed plasma 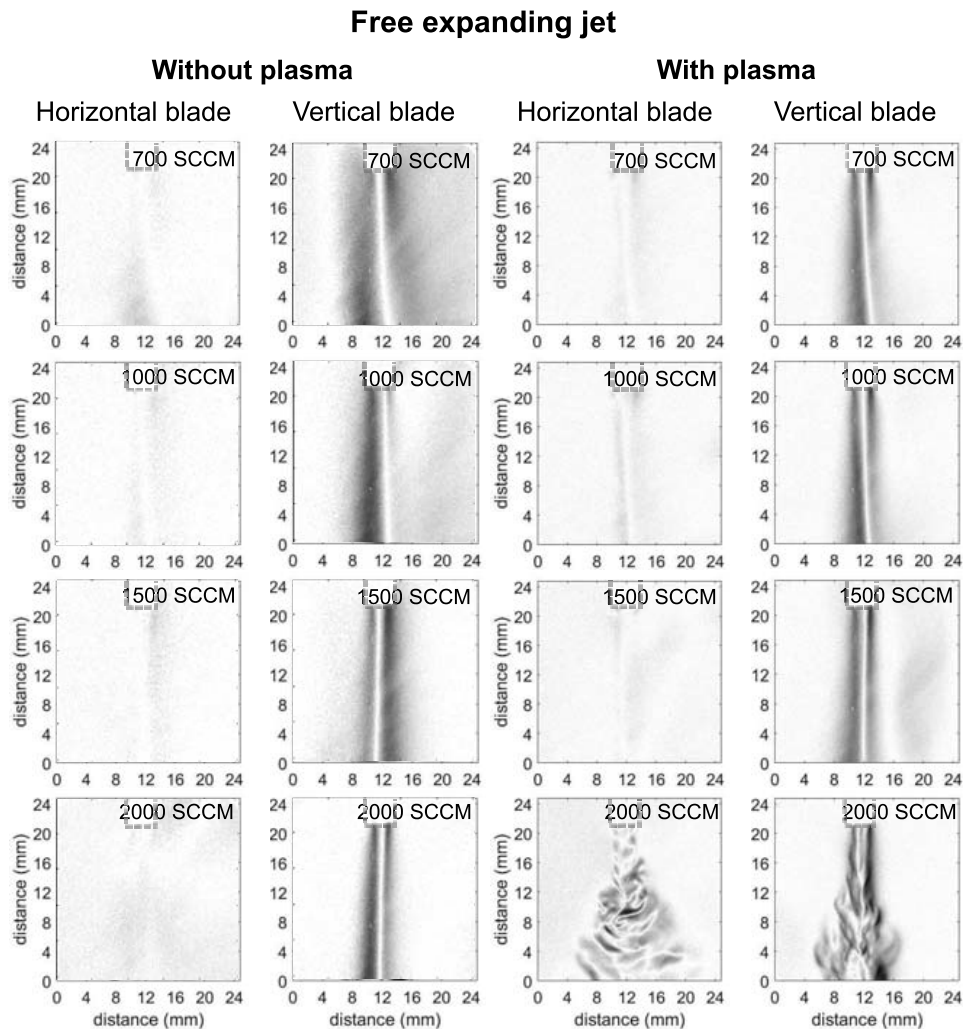jet is visible on the top in all images. Horizontally positioned blade permits visualization of the vertical gradient of the refractive index, i.e. gas mixing. Vertically positioned blade enables visualization of the changes in the refractive index in the horizontal direction.

results of this study (electric field of $26\,\text{kV cm}^{-1}$ for a $7\,\text{mm}$ distance) are in good agreement with the modeling investigation. Modification of the electrical properties of water with the addition of sodium chloride is not reflected on the electric field measurements. On the other hand, the presence of a target significantly increases the electric field strength in the area just above the target, compared to the free expanding jet, as was previously shown for a metal target [23]. At first glance, it could seem that the presence of the target and gas flow rate are of secondary importance for the discharge conditions. However, further considerations point out that the gas flow rate influences the gas composition, the medium where the ionization wave propagates. Streamer propagation is governed by the value of the first Townsend coefficient, which is determined by the gas composition. Subsequently, it is clear why gas flow rate dominantly affects electric field strength. The presence of a target changes the applied potential and the type of the target also has great influence on the electric field strength, as shown in the study of Norberg *et al* [6].

3.4. Schlieren imaging

As was mentioned earlier, the bulk of the reactive species are produced in the gas phase of the plasma jet [5]. Moreover, it was shown that the distance between the target and the plasma jet nozzle, for a fixed gas flow, affects the production of the reactive species. These facts are in line with the outcomes of this article. The electron energy, electron density and the reaction rates of the production of the active chemical species are a function of the electric field strength [17, 48]. The electric field strength in the ionization front of the streamer acts as a good candidate for the modification and comparison of different plasma jet configurations. Our previous study of the same type of jet operating without a target demonstrated that the electric field profile and length of the plume are governed to a large part by the gas mixing and the change in the molar fraction of gases induced by an increase of gas flow and the onset of turbulences and vortices [26]. The molar fraction of air in helium flow increases with an increase of distance from the capillary [26]. For low flows, this leads to a constriction of

the plasma bullet, which collapses into a point just at the liquid surface. Constriction is observed by the naked eye, while for high flows a formation of vortices and branching of the plume above the liquid surface appears. In order to visually connect electric field strength with helium flow rate and consequently helium mixing with air, a Schlieren setup is arranged.

Visualization of the fluid-dynamics of the jet both freely expanding and in configuration with a water target are presented in figures 13 and 14, respectively. The set of images are selected from among numerous recordings to reflect the overall behavior noted in every studied case. A subtraction with images obtained without flow and plasma is done in every situation to obtain the proper contrasts. In the gas phase, the visualized contrast is due to density changes because of the mixing of helium in air and possible heating. In the liquid phase, most likely the temperature is causing the density to change, creating the contrast.

The influence of the discharge on the gas flow is clearly notable for all conditions of the free expanding plasma jet, see figure 13. Namely, as the plasma jet is pointed down, the effect of buoyancy is conspicuous when the discharge is not ignited and it is especially visible for lower gas flows using the vertical blade when the mixing region is wide, which is represented by a wide gray region. The observation of the buoyancy effect for the presented configuration is in accordance with the theoretical prediction. Namely, the buoyancy can be considered as negligible if the Richardson number (R_i) is in the range of 10^{-3} or smaller, see [53] and references therein. For the free expanding plasma jet studied in this article, R_i is in the range of 0.027 for the gas flow of 700 SCCM to the 0.0033 for 2000 SCCM. Thus, the buoyancy effect could not be neglected in all our experiments. Calculated Reynolds numbers (R_e), for the same conditions are in the range of 50–144. When the gas flow is increased, the gas mixing region constricts because the dynamic pressure force exceeds the buoyancy force. For the whole examined gas flow range, the flow is laminar when the plasma is switched off. When the plasma is switched on, the mixing region constricts immediately for all flows. Thus, the force induced by the plasma has the same direction as the gas flow. Qualitative analysis of the Schlieren images recorded for the vertical blade position leads us to the conclusion that the plasma affects the flow in a similar way to an increase of the gas flow for 500 SCCM, due to the similarity of images for 2000 SCCM without plasma and 1500 SCCM with plasma. The plasma–flow interaction is more observable at a high gas flow, i.e. 2000 SCCM, when the plasma ignition induces a gas flow modification in the form of a turbulent propagating front in the gas phase. Turbulences are visible for both orientations of the blade. According to [53], the flow remains laminar for $R_e < 200$ when it comes into the transition regime and it becomes fully turbulent for $R_e > 650$. In the case of a studied plasma jet, $R_e = 200$ for a helium flow of 2770 SCCM, and thus the minimal influence of the plasma on the gas flow corresponds to the flow increase of about 800 SCCM.

When the liquid target is placed downstream from the glass tube, the gas flow induces a small dimpling effect with a diameter similar to the tube diameter, observable by the naked eye. The Taylor cone appearance described in the literature [54, 55], which could appear as a consequence of the high electric field in the streamer head in front of the liquid surface when the plasma is turned on, has not been observed, probably due to the compensation by the dimpling effect, similar to the atmospheric pressure glow discharge in a needle-to-liquid electrode configuration with a downstream helium flow [31, 32].

In the impinging configuration with a liquid target, a turbulent wave front propagating from the jet axis along the surface of the water appears and vortices can be seen close to the intersection point of the jet and surface. Similar effects have been noted with a metallic and dielectric substrate in the work of Boselli *et al* [56]. The addition of NaCl to the distilled water does not induce any apparent difference to the gas flow dynamics compared to distilled water alone. For this reason, only images displaying plasma-distilled water interaction are presented in figure 14.

The fluid dynamic instabilities and promotion of the transition of the laminar gas flow to the turbulence have been recently studied in detail [56, 57]. Due to the interaction with a liquid surface, the gas flows along the surface of the water and restrikes upstream making a mushroom-like shape, see the images using a horizontal blade position with the water. The spreading of the helium flow in radial and axial directions (horizontal and vertical blade positions, respectively) leads to an incremental expansion of this shape with an increase of the gas flow rate up to 2000 SCCM, see the dashed lines on the left side of figure 14. An interesting action of the plasma on the gas flow is also observed when the target is present. The discharge ignition expands the helium flow and keeps the mixing region spreading to a constant distance for all laminar flows, as marked by the dashed lines at the right-hand side of figure 14. The intersection of the plasma with the water results in a spreading of the sheath just above the liquid as long as there is a laminar flow, while an onset of turbulence with plasma at 2000 SCCM non-uniformly constricts this structure.

The mixing of the helium flow with air and the lateral extension of the flow above the liquid surface when plasma is formed could explain the low value of the field measured all the way to the surface for the high values of the flow. Namely, if Schlieren images for 5, 7 and 10 mm are compared (not shown here), it is clear that the lateral extension of the flow increases with an increase of the distance between the tube and the surface. This suggests that the higher slope of the electric field profile at a 7 mm relative to a 10 mm distance is due to differences in gas mixing. A similar effect of the spreading of the plasma on the surface of the water was found in the modeling of plasma jets interacting with liquid-covered tissue [7] and this is important for the production of charged aqueous species.

Images acquired with the vertical blade reveal a regular structure in the flow dynamics in the water, which resembles the structures in the gas phase and expand from the axis with an increase of the gas flow. Such behavior and structures are not found in a 100 mm-deep vessel (results not shown here), which implies a large impact on a solid surface at the bottom of the liquid layer (bottom of the vessel at around 6 mm), as can be seen with particle image velocimetry measurements in
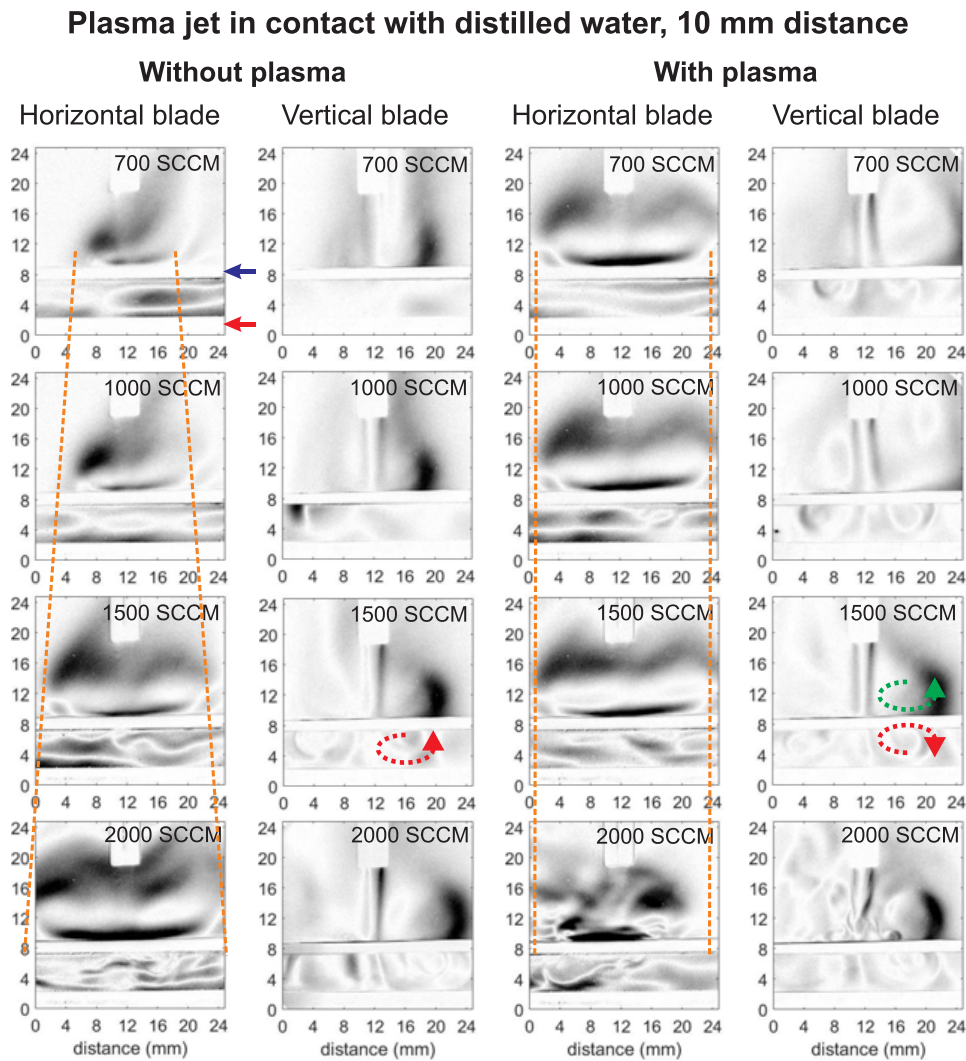
Figure 14. Schlieren images of the jet with a liquid target for different gas flows. In the first image, the blue arrow indicates the gas–liquid interface and the red arrow shows the bottom of the liquid container. Exit of the vertically installed plasma jet is visible on the top in all images.

[58]. Also, these effects in the liquid are more apparent when the water surface is at 10 mm from the tube rather than for distances of 5 and 7 mm. The helium flow alone induces water circulation in the opposite direction to the one that a gas jet would normally induce due to the friction at the interface [59], see red curved arrow in the 1500 SCCM flow figure for the jet without plasma in figure 14. The observed effect may be due to a colder helium gas that is cooling down the water at the impact point and therefore induces a sinking flow of colder water.

The movement and pattern in the liquid become much more pronounced with the ignition of the plasma. The plasma action on the flow in gas and liquid phase extends radially to the same distances. The plasma reverses the water circulation direction. The reverse of circulation direction with the discharge ignition can be either due to a higher gas flow speed at the liquid gas interface and higher friction or due to the heating of the surface at the impact point, as suggested in [59] and [60].

The nature of the plasma–flow interaction is not completely understood. There are two leading opinions about the possible mechanism of this kind of interaction. The first is the ionic wind due to the acceleration of the ions by the electric

field and the other is the acoustic wave, which starts from the heated high-voltage electrode.

In the recently published experimental study, Darny *et al* argued that the electrohydrodynamic of negative ions causes the main effect of the plasma on the helium flow [61]. This parametric study, mainly based on Schlieren imaging, revealed that the helium front expansion velocity depends on the applied voltage amplitude and on the target electrical characteristics, which suggests an ionic wind-type action mechanism. According to this study, ions are accelerated by the electric field and then they transfer their kinetic energy to the surrounding neutrals by collision. The authors found that the effective gas flow increases for negative voltage pulses, which is in agreement with the operating mechanism of plasma actuators where 97% of momentum transfer occurs in the negative voltage half cycle [62]. Indeed, the geometry of the investigated plasma gun is asymmetric, similar to the geometry of the discharge studied in this article, which is required for ionic wind generation [57, 63, 64]. Momentum transfer from the negative ions to the neutrals is much more effective than the momentum transfer from the positive ions. The ion

densities were measured by mass spectrometric methods and the plasma jets produce heavy negative ions and ion clusters with the lifetime of about 150 μs, which is three times longer than the lifetime of lighter positive ions [65, 66].

The other possible mechanism of the influence of the discharge on the gas flow may be the acoustic wave that propagates from the fast-heated tip of the high-voltage electrode. The modeling of this process showed that the powered electrode heating occurs on the time scale of voltage pulse (100 ns) and that the temperature of the tip can reach 800 °C [67]. Acoustic wave exits the tube and influences the gas flow. When the gas heating was turned off in the model, the acoustic wave and change in the flow did not develop. In contrast, including or excluding momentum transfer due to the charged species did not have a significant effect on the gas flow. The obtained effects in this article were similar to the experimentally obtained results [56, 68]. There are also experimental evidences of the shock wave emission from the high-voltage electrode of the pin to plate pulsed corona discharge [69, 70] and the modeling outcomes that are in line with these claims [71].

It is difficult to decide which mechanism is dominant and it may vary in dependence on the discharge geometry and conditions. Also, it is possible that both mechanisms contribute to the plasma–flow interaction. Thus, further, more detailed studies that will take into account different plasma jet geometries and discharge conditions are necessary in order to systematically answer these questions.

4. Conclusion

The results of the article emphasized the complexity of the plasma–liquid interaction on the plasma jet example. Using several diagnostics methods, it was shown that a slight change of the non-electrical parameters, such as the target distance and gas flow rate can completely change the nature of the discharge, such as the duration of the plasma–liquid interaction, distribution of the excited species and the value of the electric field strength in the ionization wave. The gas flow rate influence dominates over the target influence in the case of a liquid target, but the target presence is not negligible.

ICCD recordings of the discharge development revealed that the discharge interaction with the target can be elongated several times, up to 10 μs with the proper choice of flow rate and target distance, i.e. specific gas composition between the nozzle and target. High gas flows and high helium content medium in the gap decrease the production of chemical species and the electric field strength in the ionization wave.

The influence of the liquid target on the electric field in the ionization front has been studied. It is shown that just the presence of the target changes the properties of the plasma jet. The influence of the liquid target is double. It influences the gas composition and changes the potential in the gap, especially in its vicinity, which is notable in the measured electric field values. These values are in the range of 8–30 kV cm^{-1}, depending only on the gas flow and target distance, and they are in reasonable agreement with the modeling outcomes.

Schlieren imaging demonstrated strong interaction between the gas flow and the plasma itself, both for the free expanding plasma jet and the jet in contact with a liquid. A special outcome of this article is the influence of the plasma jet discharge on the mixing within the liquid.

All measurements are compared with the results of the free expanding plasma jet. This comparison leads us to the conclusion that the diagnostics of a plasma jet intended for applications should be performed during the contact with the target, because the free expanding plasma jet and the plasma jet in contact with the target represent two essentially different discharges.

ORCID iDs

Vesna V Kovačević https://orcid.org/0000-0002-8575-1668
Goran B Sretenović https://orcid.org/0000-0003-4817-4723
Elmar Slikboer https://orcid.org/0000-0002-7716-907X
Olivier Guaitella https://orcid.org/0000-0002-6509-6934
Ana Sobota https://orcid.org/0000-0003-1036-4513
Milorad M Kuraica https://orcid.org/0000-0001-8201-8500

References

[1] Lu X, Laroussi M and Puech V 2012 On atmospheric-pressure non-equilibrium plasma jets and plasma bullets *Plasma Sources Sci. Technol.* **21** 34005
[2] Lu X, Naidis G V, Laroussi M and Ostrikov K 2014 Guided ionization waves: theory and experiments *Phys. Rep.* **540** 123–66
[3] von Woedtke T, Reuter S, Masur K and Weltmann K-D 2013 Plasmas for medicine *Phys. Rep.* **530** 291–320
[4] Lu X, Naidis G V, Laroussi M, Reuter S, Graves D B and Ostrikov K 2016 Reactive species in non-equilibrium atmospheric-pressure plasmas: generation, transport, and biological effects *Phys. Rep.* **630** 1–84
[5] Gorbanev Y, O'Connell D and Chechik V 2016 Non-thermal plasma in contact with water: the origin of species *Chemistry* A **22** 3496–505
[6] Norberg S A, Johnsen E and Kushner M J 2015 Helium atmospheric pressure plasma jets touching dielectric and metal surfaces *J. Appl. Phys.* **118** 13301
[7] Norberg S A, Tian W, Johnsen E and Kushner M J 2014 Atmospheric pressure plasma jets interacting with liquid covered tissue: touching and not-touching the liquid *J. Phys. D. Appl. Phys.* **47** 475203
[8] Lindsay A, Anderson C, Slikboer E, Shannon S and Graves D 2015 Momentum, heat, and neutral mass transport in

convective atmospheric pressure plasma-liquid systems and implications for aqueous targets *J. Phys. D: Appl. Phys.* **48** 424007

[9] Sretenović G B, Krstić I B, Kovačević V V, Obradović B M and Kuraica M M M 2011 Spectroscopic measurement of electric field in atmospheric-pressure plasma jet operating in bullet mode *Appl. Phys. Lett.* **99** 161502

[10] Sobota A, Guaitella O and Garcia-Caurel E 2013 Experimentally obtained values of electric field of an atmospheric pressure plasma jet impinging on a dielectric surface *J. Phys. D: Appl. Phys.* **46** 372001

[11] Olszewski P, Wagenaars E, McKay K, Bradley J W and Walsh J L 2014 Measurement and control of the streamer head electric field in an atmospheric-pressure dielectric barrier plasma jet *Plasma Sources Sci. Technol.* **23** 15010

[12] Wu S and Lu X 2014 Two counter-propagating He plasma plumes and ignition of a third plasma plume without external applied voltage *Phys. Plasmas* **21** 23501

[13] Robert E, Darny T, Dozias S, Iseni S and Pouvesle J M 2015 New insights on the propagation of pulsed atmospheric plasma streams: from single jet to multi jet arrays *Phys. Plasmas* **22** 122007

[14] van der Schans M, Böhm P, Teunissen J, Nijdam S, IJzerman W and Czarnetzki U 2017 Electric field measurements on plasma bullets in N_2 using four-wave mixing *Plasma Sources Sci. Technol.* **26** 115006

[15] Uchida G, Nakajima A, Takenaka K, Koga K, Shiratani M and Setsuhara Y 2015 Gas flow rate dependence of the discharge characteristics of a plasma jet impinging onto the liquid surface *IEEE Trans. Plasma Sci.* **43** 4081–7

[16] Naidis G V 2011 Modelling of plasma bullet propagation along a helium jet in ambient air *J. Phys. D: Appl. Phys.* **44** 215203

[17] Boeuf J-P, Yang L L and Pitchford L C 2013 Dynamics of a guided streamer ('plasma bullet') in a helium jet in air at atmospheric pressure *J. Phys. D: Appl. Phys.* **46** 15201

[18] Breden D, Miki K and Raja L L 2011 Computational study of cold atmospheric nanosecond pulsed helium plasma jet in air *Appl. Phys. Lett.* **99** 111501

[19] Wang L, Zheng Y and Jia S 2016 Numerical study of the interaction of a helium atmospheric pressure plasma jet with a dielectric material *Phys. Plasmas* **23** 103504

[20] Breden D and Raja L L 2014 Computational study of the interaction of cold atmospheric helium plasma jets with surfaces *Plasma Sources Sci. Technol.* **23** 65020

[21] Yan W and Economou D J 2017 Gas flow rate dependence of the discharge characteristics of a helium atmospheric pressure plasma jet interacting with a substrate *J. Phys. D: Appl. Phys.* **50** 415205

[22] Jánský J, Tholin F, Bonaventura Z and Bourdon A 2010 Simulation of the discharge propagation in a capillary tube in air at atmospheric pressure *J. Phys. D: Appl. Phys.* **43** 395201

[23] Sretenović G B, Krstić I B, Kovačević V V, Obradović B M and Kuraica M M 2014 Spatio-temporally resolved electric field measurements in helium plasma jet *J. Phys. D: Appl. Phys.* **47** 102001

[24] Pechereau F, Jánský J and Bourdon A 2012 Simulation of the reignition of a discharge behind a dielectric layer in air at atmospheric pressure *Plasma Sources Sci. Technol.* **21** 55011

[25] Guaitella O and Sobota A 2015 The impingement of a kHz helium atmospheric pressure plasma jet on a dielectric surface *J. Phys. D: Appl. Phys.* **48** 255202

[26] Sobota A, Guaitella O, Sretenović G B, Krstić I B, Kovačević V V, Obrusnik A, Nguyen Y N, Zajickova L, Obradović B M and Kuraica M M 2016 Electric field measurements in a kHz-driven He jet—the influence of the gas flow speed *Plasma Sources Sci. Technol.* **25** 65026

[27] Sobota A, Guaitella O and Rousseau A 2014 The influence of the geometry and electrical characteristics on the formation of the atmospheric pressure plasma jet *Plasma Sources Sci. Technol.* **23** 25016

[28] Kuraica M M and Konjević N 1997 Electric field measurement in the cathode fall region of a glow discharge in helium *Appl. Phys. Lett.* **70** 1521–3

[29] Sretenović G B, Guaitella O, Sobota A, Krstić I B, Kovačević V V, Obradović B M and Kuraica M M 2017 Electric field measurement in the dielectric tube of helium atmospheric pressure plasma jet *J. Appl. Phys.* **121** 123304

[30] Settles G S 2001 *Schlieren and Shadowgraph Techniques: Visualizing Phenomena in Transparent Media* (Berlin: Springer)

[31] Shirai N, Nakazawa M, Ibuka S and Ishii S 2009 Atmospheric dc glow microplasmas using miniature gas flow and electrolyte cathode *Japan. J. Appl. Phys.* **48** 36002

[32] Shirai N, Ichinose K, Uchida S and Tochikubo F 2011 Influence of liquid temperature on the characteristics of an atmospheric dc glow discharge using a liquid electrode with a miniature helium flow *Plasma Sources Sci. Technol.* **20** 34013

[33] Mezei P and Cserfalvi T 2007 Electrolyte cathode atmospheric glow discharges for direct solution analysis *Appl. Spectrosc. Rev.* **42** 573–604

[34] Bruggeman P and Leys C 2009 Non-thermal plasmas in and in contact with liquids *J. Phys. D: Appl. Phys.* **42** 53001

[35] Kogelschatz U 2003 Dielectric-barrier discharges : their history, discharge physics, and industrial applications *Plasma Chem. Plasma Process.* **23** 1–46

[36] Brandenburg R *et al* 2013 Novel insights into the development of barrier discharges by advanced volume and surface diagnostics *J. Phys. D: Appl. Phys.* **46** 464015

[37] Brandenburg R 2017 Dielectric barrier discharges: progress on plasma sources and on the understanding of regimes and single filaments *Plasma Sources Sci. Technol.* **26** 53001

[38] Pearse R W B and Gaydon A G 1963 *The Identification of Molecular Spectra* (London: Whitefriars)

[39] Sretenovic G B, Krstic I B, Kovacevic V V, Obradovic B M and Kuraica M M 2012 Spectroscopic study of low-frequency helium DBD plasma jet *IEEE Trans. Plasma Sci.* **40** 2870–8

[40] Bogaczyk M, Sretenović G B and Wagner H-E 2013 Influence of the applied voltage shape on the barrier discharge operation modes in helium *Eur. Phys. J.* D **67** 212

[41] Skoblo Y É and Ivanov V A 2000 Role of metastable atoms and molecules of helium in excitation transfer to hydrogen atoms *Opt. Spectrosc.* **88** 151–7

[42] Darny T, Pouvesle J, Puech V, Douat C, Dozias S and Robert E 2017 Analysis of conductive target influence in plasma jet experiments through helium metastable and electric field measurements *Plasma Sources Sci. Technol.* **26** 45008

[43] Urabe K, Morita T, Tachibana K and Ganguly B N 2010 Investigation of discharge mechanisms in helium plasma jet at atmospheric pressure by laser spectroscopic measurements *J. Phys. D: Appl. Phys.* **43** 95201

[44] Riès D, Dilecce G, Robert E, Ambrico P F, Dozias S and Pouvesle J-M 2014 LIF and fast imaging plasma jet characterization relevant for NTP biomedical applications *J. Phys. D: Appl. Phys.* **47** 275401

[45] Norberg S A, Johnsen E and Kushner M J 2016 Helium atmospheric pressure plasma jets interacting with wet cells: delivery of electric fields *J. Phys. D: Appl. Phys.* **49** 185201

[46] Gidon D, Graves D B and Mesbah A 2017 Effective dose delivery in atmospheric pressure plasma jets for plasma medicine: a model predictive control approach *Plasma Sources Sci. Technol.* **26** 85005

J. Phys. D: Appl. Phys. **51** (2018) 065202

V V Kovačević *et al*

[47] Beebe S J, Blackmore P F, White J, Joshi R P and Schoenbach K H 2004 Nanosecond pulsed electric fields modulate cell function through intracellular signal transduction mechanisms *Physiol. Meas.* **25** 1077–93

[48] Hagelaar G J M and Pitchford L C 2005 Solving the Boltzmann equation to obtain electron transport coefficients and rate coefficients for fluid models *Plasma Sources Sci. Technol.* **14** 722–33

[49] Sretenović G B, Krstić I B, Kovačević V V, Obradović B M and Kuraica M M 2014 The isolated head model of the plasma bullet/streamer propagation: electric field-velocity relation *J. Phys. D: Appl. Phys.* **47** 355201

[50] Brandenburg R, Navrátil Z, Jánský J, St'ahel P, Trunec D and Wagner H-E 2009 The transition between different modes of barrier discharges at atmospheric pressure *J. Phys. D: Appl. Phys.* **42** 85208

[51] Hasted J B, Ritson D M and Collie C H 1948 Dielectric properties of aqueous ionic solutions. Parts I and II *J. Chem. Phys.* **16** 1–21

[52] Gavish N and Promislow K 2016 Dependence of the dielectric constant of electrolyte solutions on ionic concentration: a microfield approach *Phys. Rev.* E **94** 1–7

[53] Xiong R, Xiong Q, Nikiforov A Y, Vanraes P and Leys C 2012 Influence of helium mole fraction distribution on the properties of cold atmospheric pressure helium plasma jets *J. Appl. Phys.* **112** 33305

[54] Kawamoto H and Umezu S 2005 Electrohydrodynamic deformation of water surface in a metal pin to water plate corona discharge system *J. Phys. D: Appl. Phys.* **38** 887–94

[55] Bruggeman P, Graham L, Degroote J, Vierendeels J and Leys C 2007 Water surface deformation in strong electrical fields and its influence on electrical breakdown in a metal pin–water electrode system *J. Phys. D: Appl. Phys.* **40** 4779–86

[56] Boselli M, Colombo V, Ghedini E, Gherardi M, Laurita R, Liguori A, Sanibondi P and Stancampiano A 2014 Schlieren high-speed imaging of a nanosecond pulsed atmospheric pressure non-equilibrium plasma jet *Plasma Chem. Plasma Process.* **34** 853–69

[57] Xian Y Bin, Hasnain Qaisrani M, Yue Y F and Lu X P 2016 Discharge effects on gas flow dynamics in a plasma jet *Phys. Plasmas* **23** 103509

[58] Mededovic Thagard S, Stratton G R, Dai F, Bellona C L, Holsen T M, Bohl D G, Paek E and Dickenson E R V 2017 Plasma-based water treatment: development of a general mechanistic model to estimate the treatability of different types of contaminants *J. Phys. D: Appl. Phys.* **50** 14003

[59] Nguyen A V and Evans G M 2006 Computational fluid dynamics modelling of gas jets impinging onto liquid pools *Appl. Math. Model.* **30** 1472–84

[60] van Rens J F M, Schoof J T, Ummelen F C, van Vugt D C, Bruggeman P J and van Veldhuizen E M 2014 Induced liquid phase flow by RF Ar cold atmospheric pressure plasma jet *IEEE Trans. Plasma Sci.* **42** 2622–3

[61] Darny T, Pouvesle J-M, Fontane J, Joly L, Dozias S and Robert E 2017 Plasma action on helium flow in cold atmospheric pressure plasma jet experiments *Plasma Sources Sci. Technol.* **26** 105001

[62] Enloe C L, McHarg M G and McLaughlin T E 2008 Time-correlated force production measurements of the dielectric barrier discharge plasma aerodynamic actuator *J. Appl. Phys.* **103** 73302

[63] Johnson M J and Go D B 2017 Recent advances in electrohydrodynamic pumps operated by ionic winds: a review *Plasma Sources Sci. Technol.* **26** 103002

[64] Zhao L and Adamiak K 2005 EHD flow in air produced by electric corona discharge in pin–plate configuration *J. Electrostat.* **63** 337–50

[65] Oh J-S, Aranda-Gonzalvo Y and Bradley J W 2011 Time-resolved mass spectroscopic studies of an atmospheric-pressure helium microplasma jet *J. Phys. D: Appl. Phys.* **44** 365202

[66] McKay K, Oh J-S, Walsh J L and Bradley J W 2013 Mass spectrometric diagnosis of an atmospheric pressure helium microplasma jet *J. Phys. D: Appl. Phys.* **46** 464018

[67] Lietz A M, Johnsen E and Kushner M J 2017 Plasma-induced flow instabilities in atmospheric pressure plasma jets *Appl. Phys. Lett.* **111** 114101

[68] Qaisrani M H, Xian Y, Li C, Pei X, Ghasemi M and Lu X 2016 Study on dynamics of the influence exerted by plasma on gas flow field in non-thermal atmospheric pressure plasma jet *Phys. Plasmas* **23** 63523

[69] Ono R 2016 Optical diagnostics of reactive species in atmospheric-pressure nonthermal plasma *J. Phys. D: Appl. Phys.* **49** 83001

[70] Ono R and Oda T 2004 Visualization of streamer channels and shock waves generated by positive pulsed corona discharge using laser Schlieren method *Japan. J. Appl. Phys.* **43** 321–7

[71] Kacem S, Ducasse O, Eichwald O, Yousfi M, Meziane M, Sarrette J P and Charrada K 2013 Simulation of expansion of thermal shock and pressure waves induced by a streamer dynamics in positive DC corona discharges *IEEE Trans. Plasma Sci.* **41** 942–7